ACS OMEGA

http://pubs.acs.org/journal/acsodf

Article

Mercury Removal from Wastewater Using Cysteamine Functionalized Membranes

Mohammad Saiful Islam, Ronald J. Vogler, Sayed Mohammad Abdullah Al Hasnine, Sebastián Hernández, Nga Malekzadeh, Thomas P. Hoelen, Evan S. Hatakeyama, and Dibakar Bhattacharyya*

Cite This: *ACS Omega* 2020, 5, 22255−22267

Read Online

ACCESS | Metrics & More | Article Recommendations | Supporting Information

ABSTRACT: This study demonstrates a three-step process consisting of primary pre-filtration followed by ultrafiltration (UF) and adsorption with thiol-functionalized microfiltration membranes (thiol membranes) to effectively remove mercury sulfide nanoparticles (HgS NPs) and dissolved mercury (Hg^{2+}) from wastewater. Thiol membranes were synthesized by incorporating either cysteine (Cys) or cysteamine (CysM) precursors onto polyacrylic acid (PAA)-functionalized polyvinylidene fluoride membranes. Carbodiimide chemistry was used to cross-link thiol (−SH) groups on membranes for metal adsorption. The thiol membranes and intermediates of the synthesis were tested for permeability and long-term mercury removal using synthetic waters and industrial wastewater spiked with HgS NPs and a Hg^{2+} salt. Results show that treatment of the spiked wastewater with a UF membrane removed HgS NPs to below the method detection level (<2 ppb) for up to 12.5 h of operation. Flux reductions that occurred during the experiment were reversible by washing with water, suggesting negligible permanent fouling. Dissolved Hg^{2+} species were removed to non-detection levels by passing the UF-treated wastewater through a CysM thiol membrane. The adsorption efficiency in this long-term study (>20 h) was approximately 97%. Addition of Ca^{2+} cations reduced the adsorption efficiencies to 82% for the CysM membrane and to 40% for the Cys membrane. The inferior performance of Cys membranes may be explained by the presence of a carboxyl (−COOH) functional group in Cys, which may interfere in the adsorption process in the presence of multiple cations because of multication absorption. CysM membranes may therefore be more effective for treatment of wastewater than Cys membranes. Focused ion beam characterization of a CysM membrane cross section demonstrates that the adsorption of heavy metals is not limited to the membrane surface but takes place across the entire pore length. Experimental results for adsorptions of selected heavy metals on thiol membranes over a wide range of operating conditions could be predicted with modeling. These results show promising potential industrial applications of thiol-functionalized membranes.

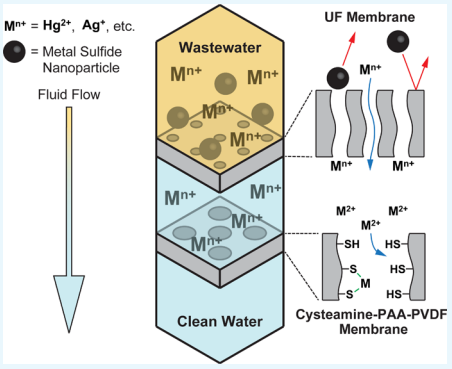

1. INTRODUCTION

Discharge of wastewaters with elevated concentrations of mercury and other heavy metals can potentially impact aquatic life and the food chain.[1−3] Depending on site-specific conditions such as mercury speciation, geochemical conditions, and the presence of labile organic matter, certain mercury species deposited in sediments can be methylated over time and potentially accumulate in benthic organisms and fish to levels of concern.[4] Development of processes for effective, sustained, and cost-effective removal of dissolved Hg, elemental Hg, and nanoparticulate HgS from various wastewaters has been a challenge to scientists and the engineering community.[5−8] A variety of physical and/or chemical treatment processes have been proposed and developed for removal of particle-bound and dissolved Hg species from wastewater.[9−12] The effectiveness of physical separation of particle-bound Hg through methods such as filtration, flotation, centrifugation, or gravity settling is typically a function of particle size and/or specific gravity. Technologies for removal of dissolved Hg species from wastewater include ion exchange, activated carbon absorption, precipitation, electrodeposition, selective liquid−liquid extraction, and membrane separation.[13−22]

The physical and chemical composition and characteristics of wastewater can be complex. The performance efficiencies of most treatment technologies highly depend on the water source (sediment, surface water, groundwater, or industrial effluent water) and water composition, including mercury speciation and concentration, water quality parameters such as

Received: May 28, 2020
Accepted: August 13, 2020
Published: August 27, 2020

https://dx.doi.org/10.1021/acsomega.0c02526
ACS Omega 2020, 5, 22255−22267

pH, redox potential, ionic composition, ionic strength, and the presence of DOM and dispersed oil.[23] Removal of mercury and other heavy metals can be associated with several of these parameters. Among the treatment processes to remove dissolved Hg from wastewater, membrane-based separation is not well explored despite offering high treatment capacities, relatively small footprints, and long-term stability suitable for full-scale operation for industrial applications.[24,25] PVDF microfiltration membranes are well studied for various separation technologies because of their high surface area and robust nature, and their surfaces are very suitable to functionalize with carboxyl (−COOH) groups.[26−32] Carboxyl groups incorporated in PVDF membranes can be activated through ethyl(dimethylaminopropyl) carbodiimide/*N*-hydroxysuccinimide (EDC/NHS) coupling.[24,33−35] The NHS−O^- functional groups formed during this process can subsequently be substituted by thiol-containing amines (organic compounds containing a basic nitrogen atom with a lone pair of electrons, e.g., R-NH_2). The resulting thiol membranes are expected to effectively absorb ionic mercury from water because of the strong propensity of thiols to bond with ionic mercury to form mercury−sulfur complexes.[11,36,37]

In a previous study, we developed a methodology to prepare thiol-functionalized membranes with a high capacity to capture selected heavy metals from synthetic wastewater.[24] The thiol membranes were synthesized by attaching either the amino acid cysteine ($C_3H_7NO_2S$, Cys) or cysteamine (or β-mercaptoethylamine (C_2H_7NS, CysM)) within the PVDF membrane by ion exchange or by EDC/NHS chemistry. The thiol functional group is a soft ligand known to react strongly with soft Lewis acids such as Ag^+ and Hg^{2+} and therefore a good candidate to remove ionic Hg^{2+} species from water.[38−41] Cys and derivatives of Cys are well known for immobilization on polyelectrolytes to separate mercury and other heavy metal ions.[11,42−45] However, its efficacy for removal of Hg^{2+} from industrial wastewater is not well documented. Further, the presence of additional carboxyl groups at the end chain of Cys could alter the adsorption efficiency in the presence of multiple cations. In this context, an alternative thiol precursor needs to be investigated for removal of Hg^{2+} from wastewater, such as CysM. The main difference between Cys and the less studied CysM is the absence of a carboxyl group in CysM. This could theoretically make CysM a more effective alternative to remove heavy metals from wastewater because relatively high concentrations of other cations (Ca^{2+}, Mg^{2+}) in wastewater may interact with the carboxyl group due to their higher reactivity compared to heavy metal cations (Hg^{2+}, Ag^+) and cause steric hindrance for Hg^{2+}−SH^- interaction.

Removing mercury from wastewater compared to synthetic water can be challenging because the complexity of the water matrix can significantly impact the solid removal and adsorption performance of a treatment process. In addition, long-term application of filtration and adsorption processes for removal of heavy metals can alter the performance of the treatment process over time. A few literature studies have evaluated mercury removal from real wastewater.[23] The overall objective of this work was to develop and evaluate a process for removal of mercury from real industrial wastewater. Under this broader objective, the specific aims of this work were to (i) establish a process to remove both HgS nanoparticles and dissolved Hg^{2+} from wastewater, (ii) evaluate the impact of cations in the wastewater on mercury removal by thiol-functionalized membranes, (iii) assess the performance of the thiol membrane for long-term mercury adsorption, and (iv) develop and validate a mathematical model to predict the performance of a thiol membrane for heavy-metal adsorption.

2. RESULTS AND DISCUSSION

Mercury removal from wastewater may be very different than removal from synthetic waters (i.e., aqueous solutions generated in the laboratory by adding chemicals to tap, deionized, or distilled water) in part because of the presence of dissolved mercury species and other dissolved salts or gases, HgS NPs, and other solids or dissolved or free phase organic materials, which can significantly impact the adsorption performance of the treatment process.[23] The wastewater composition may depend on the source of the water, e.g., sediment, surface water, ground water, or industrial wastewater, which could also alter the adsorption performance.

Long-term operation for heavy-metal adsorption can also affect the overall performance of the treatment process. The effectiveness of a water treatment process in general, or heavy-metal removal from wastewater in particular, is usually determined by a site-specific treatability study. The industrial wastewater used for this study, which was collected from a US industrial site (described in Supporting Information Section 1 (Table S1)), contained particulate Hg (HgS NPs), other particulate matter, dissolved Hg^{2+}, and a variety of dissolved salts.

A process that effectively removes both HgS NPs and dissolved mercury species from wastewater and is robust enough for long-term treatment requires multiple processing steps. Based on the quality of the industrial wastewater, we propose a three-step treatment process consisting of pre-filtration followed by ultrafiltration and membrane adsorption. The proposed treatment process is depicted in Supporting Information Section 2 (Figure S1). The first step consists of pre-filtration with a PVDF 700 microfiltration (MF) membrane to remove large particulates that could potentially foul or damage membranes in the second and third steps. The second step consists of ultrafiltration (UF) to remove HgS NPs through size exclusion. Any carryover of HgS NPs will adversely affect the removal of Hg^{2+} and membrane flux in the third step. The third step uses a thiol membrane to adsorb dissolved Hg^{2+} species. The sorption efficacy of Hg^{2+} cations using the thiol-functionalized Cys/CysM-PAA-PVDF membrane was demonstrated from synthetic water in an earlier publication by this group.[24] However, performance of the Cys/CysM-PAA-PVDF membrane for Hg^{2+} cation adsorption from wastewater was not evaluated. Here, in the third stage, a thiol membrane was used to adsorb dissolved Hg^{2+} species from industrial wastewater. In addition, the effect of the presence of other cations and long-term performance for sorption are also evaluated. Further, the effects of density of the thiol functional group, overall mass transfer resistance, adsorption of heavy metals, and residence time in the membrane pore domain are evaluated using a membrane model. The three steps are needed because carryover of particulates can cause significant flux reductions by fouling of membrane surfaces and clogging of membrane pores. The initial flux and changes in flux over time for the primary filtration step were measured using deionized ultra-filtered (DIUF) water and industrial wastewater. The flux data as well as images of the membrane and wastewater before and after the primary filtration step are provided in Supporting Information Section 3 (Figure S2) to show changes in membrane and wastewater conditions. The

https://dx.doi.org/10.1021/acsomega.0c02526
ACS Omega 2020, 5, 22255−22267

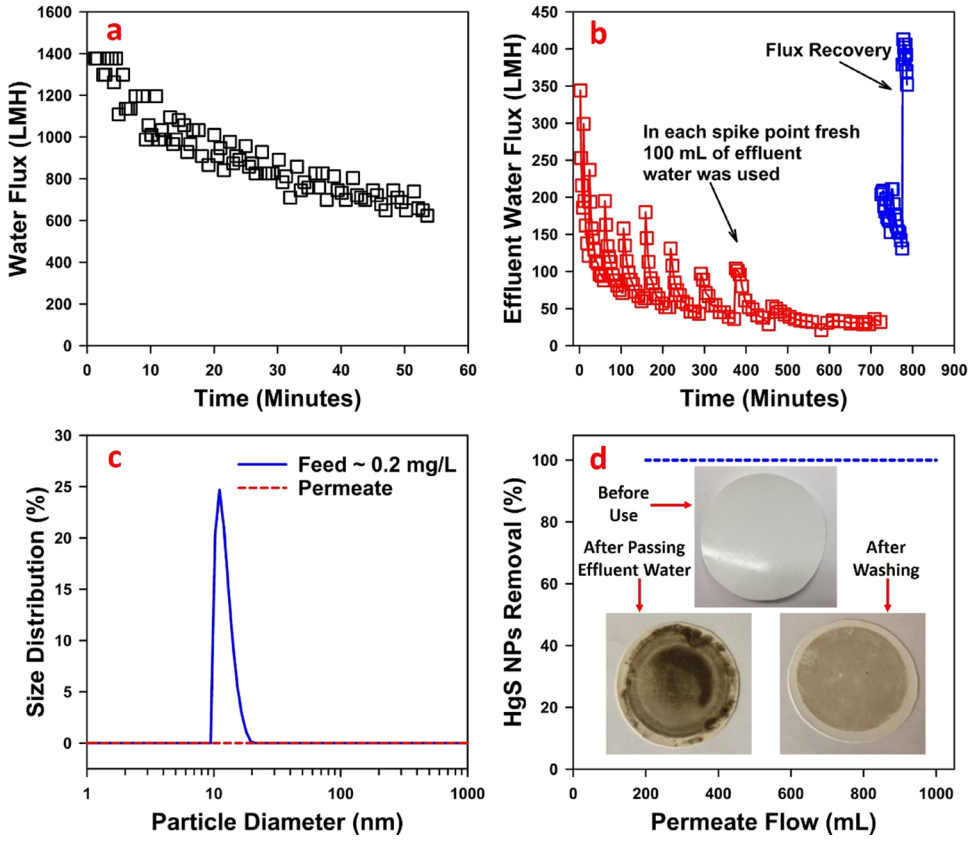

Figure 1. Flux profile for a PS35 ultrafiltration (UF) membrane by dead-end mode operation measured at 2.72 bar using (a) DIUF water and (b) wastewater (pH ~7) spiked with HgS NPs and Hg^{2+} and pre-treated by MF. A total of ~1000 mL of DIUF and wastewater was passed through a membrane in convective flow mode. Effective membrane surface area utilized was 13.2 cm^2. (c) Particle size distribution of HgS NPs in the feed and permeate measured by DLS. (d) Images of UF membrane fouling by visual observation of PS35 UF membranes, showing the color of the membrane before use, after passing spiked wastewater, and after cleaning with DIUF water. Initial concentration of HgS NPs in wastewater was approximately 200 ppb.

flux being consistent at a value of around 600 LMH ($L/m^2/h$) at atmospheric pressure and the membrane conditions after initial treatment shows removal of most of the particulates.

2.1. Removal of HgS Nanoparticles by Ultrafiltration (UF). The feed water quality can significantly affect the separation of HgS NPs in the presence of different cations (such as Na^+, Ca^{2+}, or Mg^{2+}) and organic matter.[23] The high removal rate of HgS can be adversely affected due to changes in the electrostatic repulsion between particles caused by the presence of other cations, which will have an impact on the overall ionic strength of feed water.[46−48] In addition, the presence of dissolved organic matter could affect the colloidal properties of HgS NPs.[49] This will eventually cause fouling of the membrane and affect the overall performance of the treatment process. Thus, in order to separate HgS NPs, a size exclusion process should be considered based on the size of NPs that will have zero permeation of the HgS NPs, is less susceptible to fouling, has a high processing capacity in a single pass, and is durable for long-term operation. Based on these attributes, a commercially available polysulfone ultrafiltration (UF) membrane (PS35) was selected to separate HgS NPs from wastewater. The specification of the membrane is summarized in Table S2. After primary filtration, the spiked wastewater containing both HgS and Hg^{2+} was passed through the PS35 UF membrane at 2.72 bar in dead-end mode in order to separate HgS particles. The overall performance of this filtration step in terms of DIUF water flux, spiked wastewater flux, removal of HgS NPs, fouling, and recovery of flux is demonstrated in Figure 1. The flux for DIUF water shown in Figure 1a indicates that the initial flux was approximately 1400 LMH at 2.72 bar and declined steadily to approximately 600 LMH after 55 min of operation during which 1000 mL of DIUF was passed through the filter.

The long-term flux behavior of wastewater was measured by passing 10 individual batches of 100 mL of spiked wastewater to a total of 1000 mL, which took approximately 750 min (12.5 h). The flux data are depicted in Figure 1b. The initial flux of approximately 350 LMH at 2.72 bar declined rapidly to approximately 100 LMH during the first three batches of wastewater after which the decline was relatively minor to a final flux around 35 LMH at the end of the experiment. Flux recovery was observed at the beginning of each new batch of spiked wastewater added to dead-end cells, indicated by peaks in Figure 1b. The accumulation of the HgS NPs and other particulates on top of the membrane surface is primarily responsible for the observed flux drop. The observed flux recovery after each batch of spiked wastewater may be caused by a small amount of back flow caused by changes in pressure differentials between changeouts of the batches, resulting in (partial) removal of particulates from the membrane pores. Subsequent washing of the surface of the membrane with DIUF water resulted in full flux recovery (blue line in Figure 1b), suggesting that membrane fouling under these conditions can be reversed. The distribution profile of the HgS NPs in the

https://dx.doi.org/10.1021/acsomega.0c02526
ACS Omega 2020, 5, 22255−22267

feed and permeate is depicted in Figure 1c, showing no detectable particles in the permeate by dynamic light scattering (DLS). Atomic adsorption measurements confirm removal of 200 ppb HgS NPs based on the difference between total mercury concentrations of the MF and UF permeates. This observation also suggests that no significant amount of dissolved mercury species, including organic complexes, was removed by either MF or UF membranes. The membrane was not significantly fouled as is evident from flux recovery data. The visual inspection of the UF membrane before and after washing with DIUF water, depicted in Figure 1d, supports the observation that passing wastewater through the UF membrane did not result in permanent fouling during this experiment. The calculated removal rate for 200 ppb HgS NPs using a PS35 UF membrane for this experiment is approximately 12 $mg{\cdot}m^{-2}{\cdot}h^{-1}$.

2.2. Characterization of Functionalized Membranes. Functionalization of PVDF membranes to thiol membranes using EDC/NHS chemistry consists of multiple steps, with PAA-PVDF- and NHS-PAA-PVDF-functionalized membranes as intermediates. The different functionalization steps (PAA-PVDF, NHS-PAA-PVDF, and Cys/CysM-PAA-PVDF) can be tracked by observing changes in surface charge (zeta potential) and interaction of the boundary layer of the functionalized membrane with water (surface water contact angle). Other conventional characterization techniques such as using ATR-FTIR spectra analysis was used to confirm changes in functionality of the membranes. Detailed characterization by ATR-FTIR spectra analysis is discussed in Supporting Information Section 4 (Figure S3). The surface zeta potential (ξ) of NHS-PAA-PVDF membranes and surface water contact angle (CA) profiles of various stages of a functionalized membrane is depicted in Figure 2. The surface charge (represented by zeta potential (ξ), also known as electrokinetic potential) of solid materials in contact with an aqueous solution gives an idea of charge distribution at the interface of a solid surface and the surrounding liquid to evaluate surface chemistry.[50] The NHS-PAA-PVDF membrane was selected for zeta potential (ξ) measurements because it is expected to contain both carboxylic and amine groups. The zeta potential (ξ) as a function of pH titrations between 3 and 9, depicted in Figure 2a, indicates two distinct changes in surface charge between pH 3 and 3.5 and between pH 8 and 9.5, indicating the presence of carboxyl groups and amine groups, respectively.

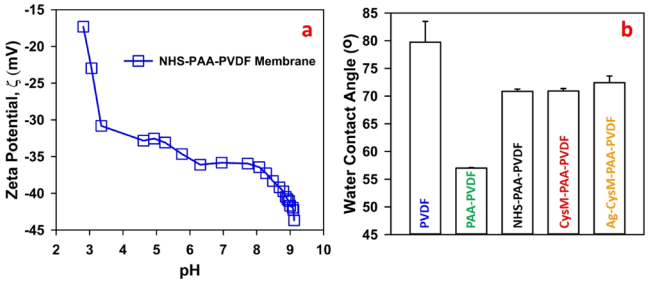

Figure 2. (a) Surface zeta potential (ξ) of an NHS-PAA-PVDF membrane (mass gain ~5%). An electrolyte solution of 0.01 M KCl was used as the background solution for pH titration. The measurement of ξ was conducted four times by flowing the electrolyte solution twice in the forward direction and twice in the reverse direction. HCl (0.05 M) and 0.05 M NaOH solutions were used for automated pH titration. Measurements of ξ for pH ranging between 2 and10 are shown. Strong declines in ξ between pH of 3 and 3.5 and between pH 8 and 9.5 are consistent with the presence of carboxyl groups and amine groups, respectively. (b) Surface water contact angle of the top surface of PVDF, PAA-PVDF, NHS-PAA-PVDF, CysM-PAA-PVDF, and Ag-CysM-PAA-PVDF (after attaching Ag) membranes. The water pH was adjusted to 6.6−6.7. A sessile drop method was used for unmodified membranes (pH ~5.5). For other membranes, air bubbles were used for captive bubble contact angle measurements at multiple locations of the samples. A volume of 1−2 μL of DI water/air droplet was placed on top of the membrane surface to measure the contact angle. A minimum of three measurements were collected at separate locations on each membrane surface. Average values and standard deviations are presented.

The sharp changes of the surface charge for those pH ranges are due to the buffering effect of the corresponding carboxyl (pH 3−3.5 ($\Delta\xi$ = 16 mV)) and amine (pH 8−9 ($\Delta\xi$ = 7 mV)) groups,[51,52] suggesting for this membrane pK_a values around 3 and 8.5. Functionalization with Cys or CysM takes place in the pore domain rather than on the surface of the membrane. Hence, measuring the surface charge of Cys- or CysM-functionalized membrane will not reflect the right information about thiol functionalization within the pores. The measured surface contact angles during each functionalization step are shown in Figure 2b. PVDF membranes are hydrophobic in nature, resulting in a water contact angle of approximately 80°, which was measured by a sessile drop method. The PAA-functionalized membranes evaluated in this study have more hydrophilic characteristics due to (i) high surface free energy that causes water droplets to spread rapidly and (ii) fast absorption of water by the PAA hydrogel, resulting in a lower water contact angle, which was measured by a captive-bubble method.[53,54] The contact angle of PAA-PVDF membranes was approximately 57° due to changes in the surface properties from hydrophobic to hydrophilic.[27] The EDC/NHS coupling resulting in the formation of NHS-PAA-PVDF membranes increased hydrophobicity, indicated by a water contact angle of 72°. This increase in hydrophobicity is caused by the coupling of an NHS functional group to the hydroxyl group on the carboxyl functional group, impacting the hydrophilic nature of the carboxyl group. The subsequent amine exchange to form CysM-PAA-PVDF membranes did not significantly impact the water contact angle, suggesting that this step did not change the hydrophobicity of the membranes. The adsorption of Ag^+, used as a model compound for heavy metals, on the CysM-PAA-PVDF membrane also did not change the contact angle significantly, implying that the transformation of thiol groups to a Ag−thiol bond has little impact on the water to solid surface interaction of the thiol membranes.

2.3. Permeance Study of Membranes during Various Stages of Thiol Functionalization. EDC/NHS coupling is well known for incorporation of amine groups by reaction with carboxyl groups through covalent bonds to form an NHS ester. The resulting O-NHS group becomes a good leaving group that can be substituted by amine containing thiol functional groups to form a stable conjugate thiol amide.[33] However, there is no reported data on permeation results when this EDC/NHS chemistry is applied on a solid substrate to incorporate the thiol functionality. The permeance behavior during each step of functionalization was evaluated. The results are shown in Figure 3. The water permeability of PAA-PVDF membranes was measured as approximately 133 LMH/bar, consistent with previous observations by this group.[27] The permeability changed significantly as a result of EDC/NHS

https://dx.doi.org/10.1021/acsomega.0c02526
ACS Omega 2020, 5, 22255−22267

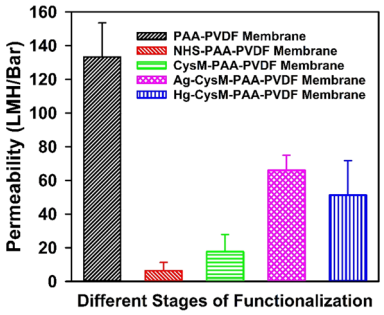

Figure 3. Permeability of PVDF membranes during various stages of functionalization. Average values and standard deviations are presented for different batches of membrane. The average mass gain of the membranes used is around 5−7%. The pH of the solution is adjusted in the range of 5.2−7.

coupling, implying a relationship to reaction mechanisms during the substitution of functional groups. A schematic of the reaction pathway is depicted in Figure S4. EDC/NHS coupling reduced the permeability from 133 LMH/bar to approximately 6 LMH/bar, presumably due to the effect of the amine functional groups (pK_a 8−9).[51] The addition of amine groups to the carboxyl groups of PAA-PVDF membranes increases the overall pK_a value from 3−4 for just the carboxyl groups to 8−9 for the amine group causes changes in the negative charge density inside the membrane pore domain, resulting in reduced permeability of NHS-PAA-PVDF membranes. An increase in the chain length of the functional groups on the membrane as a result of EDC/NHS coupling might have contributed to this strong reduction in permeability. The substitution of the NHS-O leaving group with thiol-containing amine groups with pK_a values similar to those of NHS groups increased the permeability of the CysM-PAA-PVDF membrane by approximately 3-fold to ∼17 LMH/bar. This is likely caused by a decrease in the negative charge density in membrane pores. Here, one natural concern comes in the context of low permeability in that it is possible to remove heavy metal ions using a nanofiltration (NF) membrane. However, the NF membrane will generate a high mercury wastewater stream with a significant volume (retentate stream), which may require further treatment. Heavy-metal sorption using the thiol-functionalized membrane will minimize the mercury waste to a small solid waste stream. These thiol-functionalized membranes are very effective at adsorbing heavy metals from the wastewater stream even with a very low concentration (ppb range) of mercury ions. Adsorption of Ag^+ and Hg^{2+} cations on thiol membranes increased the permeability of the membrane to 66 LMH/bar and 51 LMH/bar, respectively. This increase of permeability is presumably caused by charge neutralization in membrane pores through the adsorption of heavy metals. The theoretical capacity of the membranes to remove Hg^{2+} is approximately half of the capacity for the removal of Ag^+ because the majority of Hg^{2+} ions are expected to attach to two thiol groups. The expected initial permeability during heavy-metal adsorption should be close to the permeability of the PAA-PVDF membrane. The adsorbed metals could cross-link with thiol groups, resulting in reduced permeability.

2.4. Removal of Dissolved Hg^{2+} by the CysM-PAA-PVDF Membrane and Long-Term Performance Study. A thiol membrane was used to adsorb dissolved Hg^{2+} after removal of HgS NPs, and other particles from wastewater were adsorbed by a UF membrane. The efficacy of thiol membranes to adsorb heavy metals from synthetic water has been established in a previous study by this group.[24] The adsorption capacity of the thiol-functionalized membrane was quantified and compared with many traditional sorption materials used for Hg^{2+} removal and was reported also in the previous study.[24] The source of wastewater, concentration of dissolved Hg^{2+}, and water quality parameters (e.g., pH, types of other cations present) can have a strong impact on the membrane adsorption efficiency.[23] The hydrolysis or complexation of Hg^{2+} cations could also affect the adsorption process, as Hg^{2+} hydrolyzes readily in a wide range of pH values to form a variety of complexes with organic and inorganic ligands.[55,56] Long-term operation for removing Hg^{2+} by CysM-PAA-PVDF membranes will also affect the adsorption efficiency. The long-term adsorption performance of a CysM-PAA-PVDF membrane to remove Hg^{2+} from UF-filtered wastewater is depicted in Figure 4. The flux pattern during sorption of Hg^{2+} by a thiol membrane is shown in Figure 4a. Approximately 1700 mL of wastewater was processed by the membrane for a period of 1250 min (20.8 h) at 2.72 bar. The wastewater flux was reduced by 8-fold to approximately 25 LMH during the course of the experiment. Several factors may have caused or contributed to this flux reduction. Adsorption of Hg^{2+} cations

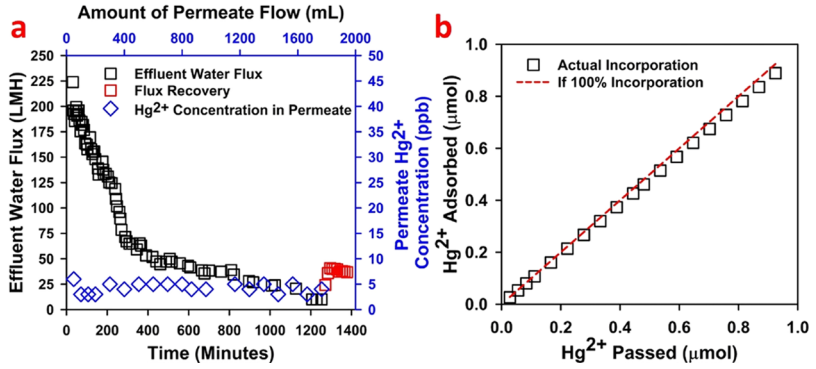

Figure 4. Long-term Hg^{2+} adsorption study on the CysM-PAA-PVDF membrane. A total of ∼1700 mL of spiked wastewater was passed through the membrane in convective flow mode at 2.72 bar. Initial concentration of Hg^{2+} was approximately 110 ppb. Membrane surface area was 13.2 cm^2. The test pressure was 2.72 bar. (a) Flux pattern of spiked wastewater and flux recovery after the adsorption study are shown on the primary (left) y axis and the remaining dissolved Hg^{2+} concentration in the permeate is shown on the secondary (right) y axis in 1300 min of operation. (b) Long-term Hg^{2+} adsorption performance (efficiency) of the CysM-PAA-PVDF membrane.

https://dx.doi.org/10.1021/acsomega.0c02526
ACS Omega 2020, 5, 22255−22267

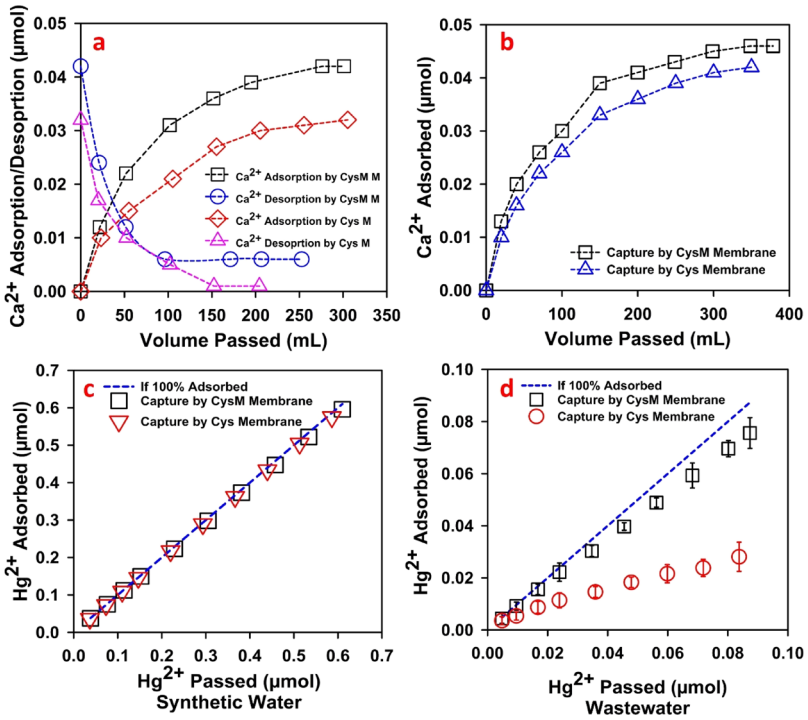

Figure 5. Effect of the presence of Ca^{2+} cations in synthetic and wastewater on Hg^{2+} adsorption by thiol membranes (Cys/CysM-PAA-PVDF). (a) Adsorption and desorption profiles of Ca^{2+} in thiol membranes from synthetic water with an initial Ca^{2+} concentration of around 30 ppm. (b) Adsorption profile of Ca^{2+} from the wastewater with the addition of Hg^{2+}, and Ca^{2+} ions are to make a total feed concentration of approximately 50 ppb Hg^{2+} and 70 ppm Ca^{2+}. (c) Adsorption of Hg^{2+} by thiol membranes from synthetic water with an initial Hg^{2+} concentration of ~150 ppb. (d) Adsorption profile of Hg^{2+} from spiked wastewater in the presence of Ca^{2+} cations for both thiol membranes. Initial concentration of Hg^{2+} of ~50 ppb. The spiked wastewater pH was around 6.5−7. The mass gain of all the membranes used for this study was in the range of 5−8%.

may have led to a reduction in the accessibility of free thiol groups in the membrane pore domain. Hg^{2+} cations attached to surface thiol groups may also have cross-linked with the existing functionalized polymer, resulting in a reduction of pore channel sizes or complete blockage of pores. In addition, the presence of other cations such as Na^{+}, Ca^{2+}, and Mg^{2+}, which are present at concentration orders of magnitude higher than Hg^{2+} but have a lower affinity to thiols, may have participated in the adsorption, leading to a drop in effluent flux over time. No visible fouling of the CysM-PAA-PVDF membrane occurred during treatment of the UF-filtered wastewater. However, washing of the membrane with DIUF after completion of the experiment helped to recover the flux to a value of 50 LMH at 2.72 bar, shown in red squares in Figure 4a. The remaining dissolved Hg^{2+} cation concentration in the permeate is shown on the secondary (right) *y* axis in Figure 4a. The remaining dissolved Hg^{2+} cation concentration in wastewater is in the range of 3−4 ppb, which is close to the EPA guideline for mercury in drinking water.[57] Adding a second CysM-PAA-PVDF membrane in the series may remove additional Hg^{2+} cations from permeate, potentially to significantly below EPA drinking water specifications. Additional adsorption−desorption of heavy metals (Ag^{+} and Hg^{2+}) on a PAA-PVDF membrane is described in Supporting Information Section 6 (Figure S5). These results support the hypothesis that the metal adsorption mechanism by thiol membranes involves covalent bonds, which limits desorption from the functionalized membrane.[24] The adsorption efficiency of heavy metals on the thiol membrane is further described in detail in Supporting Information Section 7 (Figure S6). This study confirms that removal of all dissolved heavy metal cations is not a realistic expectation for any industrial application. Pore channeling, reduced accessibility to thiol groups in the pore vicinity, and fouling from wastewater constituents eventually limit the adsorption efficiency. The adsorption efficiency in this long-term study is around 97%, as depicted in Figure 4b, confirming the effectiveness of CysM-PAA-PVDF membranes for removal of Hg^{2+} cations from wastewater.

2.5. Effect of the Presence of Ca^{2+} Cations in Wastewater on Hg^{2+} Adsorption by Thiol-Functionalized Membranes. Due to preferential cation adsorption, the presence of relatively high concentrations of common cations such as Na^{+}, Ca^{2+}, and Mg^{2+} in wastewater could reduce the sorption efficiency for soft Lewis acids with a strong affinity to thiols, specifically Ag^{+} and Hg^{2+}.[23,55] The presence of dissolved salts in wastewater results in a specific ionic strength, which causes multicationic adsorption.[23] The impact of Ca^{2+} cations on the adsorption of Hg^{2+} efficiency of Cys and CysM thiol membranes was evaluated using synthetic water containing Ca^{2+} and Hg^{2+} salts and with wastewater spiked with Ca^{2+} and Hg^{2+}. Results are depicted in Figure 5.

In this study, Ca^{2+} was chosen due to its presence in sample wastewater (see Table S1) and its location in the activity series compared to Ag^{+} and Hg^{2+} cations.[55] Initially, an adsorption−desorption study of Ca^{2+} cations on Cys-PAA-PVDF and CysM-PAA-PVDF membranes was conducted. The results of adsorption−desorption of Ca^{2+} cations using thiol membranes (Cys/CysM-PAA-PVDF) are shown in Figure 5a. A 30 ppm Ca^{2+} solution was prepared using $CaCl_2$ salt with DIUF water (synthetic water). The resulting pH was approximately 5.8. This solution was passed through a membrane by convective

https://dx.doi.org/10.1021/acsomega.0c02526
ACS Omega 2020, 5, 22255−22267

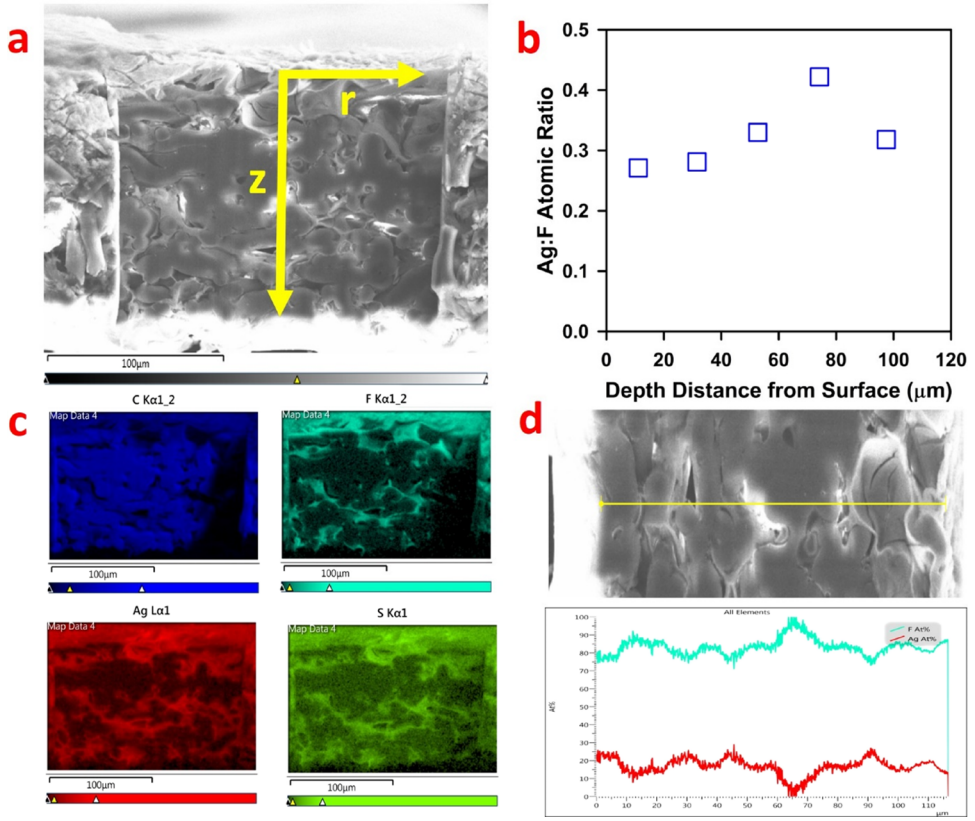

Figure 6. Characterization of the cross section of the CysM-PAA-PVDF membrane using the FIB instrument to assess the elemental composition after adsorption of Ag as a model compound. The FIB was used to prepare the entire cross section (∼120 μm) with an ion beam (2.5−6 nm), ensuring minimum damage of the sample. (a) Sample of the whole membrane cross section. The smooth area in the center was removed by the FIB, and the elemental composition is assessed in both the z and r direction. (b) Ag to F atomic ratio in different depths of the membrane, confirming an almost even adsorption of Ag^+ cations across the whole cross section (i.e., the whole pore) of the membrane. F is used as a standard as it is homogeneously distributed in the PVDF membrane. (c) Distribution profile of atomic C, F, Ag, and S across the entire cross section from the top surface is demonstrated. Ag (red) and S (green) are almost evenly distributed confirming that all the thiol (−SH) sites are utilized. (d) Line scan data of F and Ag atomic percentage in the r direction at a distance of 53 μm from the top surface.

flow at 1 bar followed by a low pH (∼2.5) solution to desorb the Ca^{2+} cations. The results, depicted in Figure 5a, confirm that the majority of Ca^{2+} was leached out of both membranes during the desorption study. The same sets of membranes were subsequently used to treat wastewater containing approximately 50 ppb Hg^{2+} and 70 ppm Ca^{2+} cations. The Ca^{2+} adsorption profile for these wastewater samples is shown in Figure 5b, indicating that the CysM membranes adsorbed approximately 8% more Ca^{2+} than the Cys membrane. Figure 5c depicts the adsorption profile of Hg^{2+} from synthetic water that contained 150 ppb Hg^{2+} (prepared by dissolving $Hg(NO_3)_2{\cdot}xH_2O$ (x = 1−2) salt in DIUF water). The adsorption efficiency is similar (∼98%) for both Cys-PAA-PVDF and CysM-PAA-PVDF membranes. In contrast to the result of Figure 5c, the adsorption of Hg^{2+} cations is significantly affected by the presence of Ca^{2+} cations in wastewater, as shown in Figure 5d. For CysM-functionalized membranes, the presence of Ca^{2+} reduces Hg^{2+} adsorption from 97.64 to 82% because both cations were adsorbed to the membrane. In comparison, for Cys-functionalized membranes, the adsorption dropped from 98 to 40%. This is because all thiol groups attached using Cys on the membrane pore domain have an additional carboxyl group in the functional chain. The Ca^{2+} cations have a high affinity in the charge domain of membrane pores to the carboxyl group and hinder the covalent association of Hg^{2+} cations to thiol groups, as demonstrated in Figure 5d. In the literature, the use of Cys and its derivatives to adsorb Hg^{2+} is a common trend and corresponding adsorption results are based only on Hg^{2+} removal from synthetic water.[5,22,37] Although it is clear that the presence of Ca^{2+} cations decreases the adsorption of Hg^{2+} cations, it does not demonstrate the selective sorption preference for either of these cations. The wastewater used in this experiment has Ca^{2+} concentration in the ppm range, and that of Hg^{2+} is in the ppb range. Thus, there is always a high concentration of Ca^{2+} cations while adsorption takes place. However, it is difficult to conclude which cations get preference. Our understanding is both cations got adsorbed simultaneously as both carboxylic group (−COOH) and thiol (−SH) groups are at the end chain of the cysteine (Cys) membrane. The presence of other cations could result in reduced adsorption of heavy metals such as Ag^+ and Hg^{2+} wastewater. In this context, CysM might be the preferred alternative for heavy-metal adsorption due to its high adsorption in the presence of other cations.

2.6. Characterization of the Depth Profile of the Thiol-Functionalized Membrane after Heavy-Metal Capture. In order to confirm that the adsorption of Ag^+ and Hg^{2+} on the CysM-PAA-PVDF membrane occurs across the pore depth and not only on the surface of the membrane, the cross section of the membrane was characterized by FIB characterization, depicted in Figure 6. The cross section of the membrane was milled using the FIB instrument using the

https://dx.doi.org/10.1021/acsomega.0c02526
ACS Omega 2020, 5, 22255−22267

technique mentioned elsewhere.[26] This method of characterization allows for precise slices with smooth surfaces for characterization inside the membrane pores. Only adsorption of Ag^+ on the CysM-PAA-PVDF membrane was characterized to avoid contamination of the FIB sample chamber by Hg^{2+} adsorbed membranes. In Figure 6a, the whole cross section of the sample membrane is visible, which is milled along the r and z directions. In Figure 6b, the atomic ratio of Ag to F at different depths in the z direction of the membrane demonstrates a relatively even adsorption of Ag^+ cations across the entire cross section (i.e., the whole pore) of the membrane. The distribution of atomic C, F, S, and Ag in the milled area is shown in Figure 6c. This observation is consistent with the literature describing membranes for other applications.[58,59] The coexistence of Ag and S in the same location of the membrane cross section, shown in Figure 6c, suggests the reaction of thiol groups to Ag in a 1 to 1 molar ratio (Ag is shown in red and S in green). Another distinct observation is that S and Ag are concentrated on the circumferences of pore mouths. This suggests that the pores are not blocked due to thiol functionalization using CysM but that thiol functionalization takes place across the pore walls of the PAA-PVDF membrane. The line scan data of F and Ag atomic percentage in the r direction at a distance of 53 μm from the membrane top surface, as shown in Figure 6d, suggests a homogeneous distribution ratio of F and Ag. In addition, the XPS results after Hg^{2+} adsorption by the CysM-PAA-PVDF membrane is discussed in detail in Supporting Information Section 8 (Figure S7). Also, the EDX scanning results for the top surface of the CysM-PAA-PVDF membrane after adsorption of Ag^+ cations from synthetic water are depicted in Supporting Information Section 9 (Figure S8) and summarized in Table S3. This detail characterization of the cross section of the CysM-PAA-PVDF membrane by FIB characterization demonstrates that the adsorption of heavy metals is not only a surface phenomenon but occurred across the entire length of the membrane pores.

2.7. Mathematical Model to Predict the Breakthrough Profile for Adsorption of Heavy Metals on the Thiol-Functionalized Membrane. For industrial application, a membrane model with similar attributes to the thiol membrane used for experimental studies can be used to predict heavy-metal adsorption breakthrough profiles to evaluate the life span of the operation. A well-defined model can assist to optimize the wastewater flux, adjust the concentration profile, calculate the life span of the membrane, and predict performance efficiency of adsorption. In this regard, a thiol membrane was modeled to predict the adsorption profile of heavy metal cations in the membrane. From the experimental study, the adsorption is linear with time, and the membrane model can be considered a one-dimensional unsteady state problem where the adsorption is taking place only in the direction of pore length.[44,60] In order to obtain a realistic model of the adsorption to match the experimental results, a Ag^+ cation adsorption study was conducted because it attaches with thiol groups in a 1:1 molar ratio. The membrane model can be described in terms of three different phases: (i) inert polymer phase ($Ø_{PVDF}$), (ii) thiol-functionalized phase ($Ø_{SH\text{-}PAA}$), and (iii) aqueous Ag^+ cation solution phase occupying part of the free volume fraction of the membrane ($Ø_{free\ space}$). This is a modification of our previously published model for mixed-matrix membranes containing thiol-functionalized silica particles.[44] The schematic of the model membrane is shown in Figure 7a as a combination of the three phases.

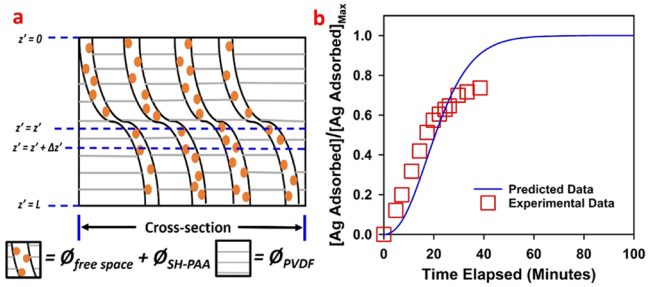

Figure 7. (a) Schematic representation of the cross section of the CysM-PAA-PVDF membrane for mathematical modeling. (b) Comparison of experimental and predicted data for the breakthrough profile for Ag^+ cation adsorption on the thiol membrane. Here, Ag used as a model compound.

The following terminology is used for the model:

$$Ø_{pore} = Ø_{free\ space} + Ø_{SH-PAA} \quad (1)$$

$Ø_{pore}$ indicates the pore volume fraction and $Ø_{PVDF}$ means the PVDF volume fraction.

Here,

$$Ø_{pore} + Ø_{PVDF} = 1 \quad (2)$$

C' is the concentration of Ag^+ in the liquid phase (moles of Ag^+/m^3 of liquid), q' is the concentration of silver in the SH-PAA layer (moles of Ag^+/m^3 of SH-PAA layer), q_{eq} is the maximum concentration of silver in the PAA-SH layer for C' (moles of Ag^+/m^3 of SH-PAA layer), J_W is the membrane water flux (m/s), t' is the time (s), and z' is the distance down the membrane thickness (m).

All quantities used in the model are initially expressed in SI units. The quantities are subsequently converted to suitable units for comparison and discussion of the experimental and predicted results. The partial differential equations (PDEs) governing linear adsorption are described by eqs 3 and 4.[60] Equation 3 is a mass balance of Ag^+ on the liquid phase, and eq 4 is the mass balance of Ag^+ on the stationary phase (SH-PAA).

A mass balance of Ag^+ in the liquid phase over an element shown in Figure 7a yields

$$Ø_{free\ space}\frac{\partial C'}{\partial t'} + J_W\frac{\partial C'}{\partial z'} + (1 - Ø_{PVDF} - Ø_{free\ space})\frac{\partial q'}{\partial t'} = 0 \quad (3)$$

A mass balance of Ag^+ in the stationary phase (SH-PAA) will consequently derive

$$\frac{\partial q'}{\partial t'} = K(q_{eq} - q') \quad (4)$$

where K is the mass transfer coefficient of Ag^+ into the stationary phase (SH-PAA). The initial boundary conditions are

$$C'(0, t') = C_0,\ q'(z',0) = 0,\ AC'(z',0) = 0$$

For this system, the axial diffusion can be neglected as compared to axial convection. To solve eqs 3 and 4, the following linear relationship between q_{eq} and C' is assumed:

https://dx.doi.org/10.1021/acsomega.0c02526
ACS Omega 2020, 5, 22255−22267

$$q'_{eq} = \gamma C' \tag{5}$$

Here, γ is the silver−thiol affinity constant. In this model, γ is a function of pore density of thiol groups.[44] Substituting eq 5 into eq 4 generates

$$\frac{\partial q'}{\partial t'} = K(\gamma C' - q') \tag{6}$$

The above equation can be made dimensionless by defining the following variables as:

$$C = \frac{C'}{C_0},\ q = \frac{q'}{q_\infty},\ z = \frac{z'}{L},\ t = \frac{t'}{T_S}$$

where C_0 is the inlet feed concentration of Ag^+ (mol of Ag^+/m^3); q_∞ is the maximum Ag^+ capture (mol of Ag/m^3 of SH-PAA); L is the membrane thickness (m); and T_S is the time at which breakthrough of Ag^+ adsorption was observed, and the experiment was terminated (s).

The breakthrough for Ag^+ adsorption can vary depending on the thickness of the thiol-functionalized layer on the membrane, the concentration of the heavy metal solution, and the residence time.

The final dimensionless system of the initial PDE (eqs 3 and 4) consists of two unsteady state partial differential equations:

$$\frac{\varnothing_{\text{free space}} L}{J_W T_s}\frac{\partial C}{\partial t} + \frac{\partial C}{\partial z} + (1 - \varnothing_{PVDF} - \varnothing_{\text{free space}})\frac{KL}{J_W}\left(\gamma C - q\frac{q_\infty}{C_0}\right) = 0 \tag{7}$$

and

$$\frac{\partial q}{\partial t} = \frac{KT_S C_0}{q_\infty}\left(\gamma C - q\frac{q_\infty}{C_0}\right) \tag{8}$$

The COMSOL Multiphysics 5.4 software platform was used to solve eqs 7 and 8. Multiphysics convection−diffusion transient state analysis was applied to the one-dimensional domain.[60] The model parameters are mostly obtained from the experimental study and are as follows: C_0 = feed of Ag^+ cation concentration = 0.85 mol/m^3 (~90 ppm); $L = 120 \times 10^{-6}$ m (120 μm) (membrane thickness along with the backing material measured by the FIB instrument); $J_W = 6.93 \times 10^{-5}$ m/s (~250 LMH); $\varnothing_{pore}$ = 0.52 (based on membrane data sheet); $\varnothing_{PAA\text{-}SH}$ = 0.35; and γ = 5021. Both $\varnothing_{SH\text{-}PAA}$ and γ are calculated based on a previous study.[27,44] In eq 7, an artificial diffusion term is added to get a stable numerical solution. A diffusivity value of 1.80×10^{-9} m^2/s for $AgNO_3$ was used for calculations based on the reported literature data.[61] The only unknown parameter remaining was the volumetric mass transfer coefficient (K), which was used as an adjustable parameter to match the predicted data with experimental data. Mass transfer coefficients for packed columns (gas−liquid) typically range between 0.005 and 0.02 s^{-1}.[62] A K value of 0.0058 s^{-1} is therefore well-fitted in the range.[44] The predicted and experimental breakthrough curves are shown in Figure 7b. The breakthrough of Ag^+ cation adsorption on membranes appears around the same elapsed time (~38 min) of operation for both predicted and experimental studies. However, for our experimental study, pore channeling, lower accessibility to thiol groups on pore vicinity, and fouling limits the adsorption efficiency to ~80%. The rational agreement between predicted and experimental data in this study anticipates that the membrane model is helpful to predict experimental results over a wide range of operating conditions and parameters like thiol loading in terms of membrane mass gain, wastewater flux, heavy-metal adsorption capacity, wastewater metal concentration, and membrane thickness. More broadly, this model may be used to model other membrane adsorption processes.

3. CONCLUSIONS

A commercially available ultrafiltration (UF) membrane in combination with in-house fabricated thiol membranes can remove HgS NPs and adsorb dissolved Hg^{2+} from wastewaters. Over 12 h of continuous operation shows consistent removal of ~200 ppb HgS NPs from wastewater by UF membrane filtration. While membrane fouling occurred, it was demonstrated that a water wash could recover the flux. Dissolved Hg^{2+} from UF-filtered wastewater was effectively removed by a CysM-PAA-PVDF membrane. Long-term (1250 min) wastewater treatment with an adsorption efficiency of 97% suggesting an in-house functionalized membrane is well suited for mercury removal applications. The presence of Ca^{2+} cations reduced the adsorption efficiency to 82% for the CysM-PAA-PVDF membrane and to 40% for Cys-PAA-PVDF membranes, suggesting that CysM thiol membranes will be superior for removal of mercury from wastewater compared to Cys thiol membranes. Characterization of the cross section of the CysM-PAA-PVDF membrane by FIB characterization confirmed that the adsorption takes place across the entire pore length and is not limited to the membrane surface. Mathematical modeling of heavy-metal adsorption on thiol membranes was effective in predicting experimental results over a wide range of operating conditions, suggesting a high potential for commercialization.

4. MATERIALS AND METHODS

4.1. Materials. All chemicals in this study were used as received and are listed in Supporting Information Section 10.

4.2. Materials Characterization. Thiol membranes were characterized using attenuated total reflectance Fourier transform infrared spectroscopy (ATR-FTIR), X-ray photoelectron spectroscopy (XPS), total organic carbon (TOC) analysis, scanning electron microscopy (SEM), focused ion beam SEM (FIB-SEM), energy-dispersive X-ray spectroscopy (EDS), contact angle measurements, and surface zeta potential measurement instruments. ATR-FTIR (Nicolet iS50 FT-IR spectrometer, Thermo Scientific) was used to verify the membrane synthesis at various stages of functionalization of the PVDF membrane. XPS (Thermo Scientific K-alpha XPS System) was used to verify membrane synthesis and metal adsorption across the membrane cross section. TOC analysis was performed using a TOC-5000A (Shimadzu) instrument to verify membrane synthesis by calculating carbon balance during EDC/NHS functionalization and Cys or CysM incorporation. Surface morphology (membrane pore size and porosity) of the functionalized membrane was recorded by SEM (Hitachi S-4300). Membrane pore size and surface porosity (ratio of the pore area to the total membrane area) were determined using ImageJ software. Contact angles were measured using a Krüss drop shape analyzer instrument (DSA100) to evaluate potential changes in hydrophobicity or hydrophilicity of the surface of the functionalized membranes. Zeta potential was analyzed using an Anton-Paar SurPASS electrokinetic analyzer to verify changes in surface charge due

https://dx.doi.org/10.1021/acsomega.0c02526
ACS Omega 2020, 5, 22255−22267

to incorporation of carboxyl and thiol functional groups in membranes. The distribution of heavy metals was measured both on the surface and inside the pores of the thiol membrane after preparing a lamella from the membrane using a FIB-SEM (FEI Helios Nanolab 660) instrument. TEM (JEOL 2010F) coupled with energy-dispersive X-ray spectroscopy (EDS) and electron energy loss spectroscopy (EELS) were used to determine the captured heavy-metal distribution across the cross section of the thiol membrane. Light scattering (Litesizer 500, Anton Paar) for particle analysis was used to determine the size distribution and particle diameter of HgS NPs.

4.3. Functionalization of PVDF 700 Membranes with PAA. Thiol membranes were prepared by incorporating carboxyl groups on commercially available PVDF membranes and subsequently attaching amines with thiol functional groups to the carboxyl functionalized membrane. PVDF 700 membranes were functionalized with PAA using a protocol described previously.[27] The information of the commercial PVDF 700 membrane and degree of polymerization grafting was discussed in earlier literature studies published by this group.[27,63] Briefly, the membrane samples were weighed and submersed in methanol to clean the pores. An aqueous potassium persulfate (KPS) initiator was combined with an aqueous solution containing acrylic acid (AA) and a *N*,*N*′-methylenebisacrylamide (MBA) cross-linker to form an aqueous polymeric liquid containing 5−8 wt % AA, MBA (1 mol % of AA), and KPS (1 mol % of AA). This mixture was passed through the top and back surface of the cleaned membranes using a vacuum pump. Excess polymeric liquid was dried off from the membrane samples by evaporation. Finally, the wet membranes were wrapped with plastic sheets, placed between glass/Teflon plates, and dried in an oven for 1−2 h at around 70−80 °C under vacuum to generate PAA-functionalized PVDF (PAA-PVDF) membranes.

4.4. Functionalization of PAA-PVDF Membranes with Thiol Groups. The PAA-PVDF membranes were functionalized with EDC/NHS and thiol solutions to generate Cys- and CysM-PAA-PVDF membranes (collectively referred to as thiol membranes). The thiol groups enable a membrane to capture heavy metals from water that passes through the membrane by chemisorption. The EDC/NHS and Cys/CysM thiol functionalization was performed by a modification of our protocol described elsewhere.[24] A schematic of the thiol functionalization is shown in Supporting Information Section 5 (Figure S4). A solution with a pH of 6.3 containing 5.0 mM EDC, 5.0 mM NHS, and 450 mM NaCl was passed through a PAA-PVDF membrane at a pressure of 6.9 ± 0.3 bar in convective flow mode using a dead-end filtration cell. The resulting NHS-PAA-PVDF membrane was rinsed with DI water at the same pressure. A solution of 1.0 g/L of either Cys or CysM solution (pH 7.5) was subsequently passed through the NHS-PAA-PVDF membranes to incorporate thiol groups in the membrane. The resulting thiol membranes were rinsed with DI water. The amount of Cys or CysM used to functionalize this membrane is very low, which is equivalent to ∼12 g/m^2 PVDF for Cys and ∼8 g/m^2 PVDF of CysM, with an average mass gain of the membrane in the range of 7−8%. During this process, the membranes were stored at 4−5 °C when not in use. The flux and volumes of the feed, permeate, and retentate were recorded throughout the functionalization processes, and the liquids were analyzed by TOC to calculate the degree of thiol incorporation by carbon balance. Conversion of PAA-PVDF membranes to NHS-PAA-PVDF membranes during EDC/NHS functionalization and corresponding flux pattern is shown in Supporting Information Section 11 (Figure S9). Progressive attachment of thiol groups in NHS-PAA-PVDF membranes by CysM incorporation and flux pattern is shown in Supporting Information Section 12 (Figure S10). In order to prepare the thiol-functionalized membrane using precursor Cys and CysM, no solvents were used to prepare the solution. All chemical solutions are prepared in water from the beginning to the end of the functionalization. Thus, releasing of toxic organic solvents during their fabrication is not associated with this functionalization method. Further, measurement of Cys or CysM concentration of the permeate stream was conducted while performing the adsorption experiment. No leaching of Cys or CysM was observed in this process, which we reported in our earlier literature.[24]

4.5. Permeability Measurements of Membranes and Its Impact on Functionalization. Changes in ionic strength of the solution permeating a carboxyl-functionalized PVDF membrane can cause charge−charge repulsion/attraction in polymer layers incorporated in membrane pores, resulting in swelling or shrinkage of pores and an associated change in permeability.[64,65] Observation of the changes in transport properties, such as water permeability, after each functionalization step provides a qualitative assessment of the success of each functionalization step. Thus, the functionality of thiol membranes can be evaluated by measuring the permeability of the unaltered PVDF membrane, the PAA-PVDF membrane, the PAA-PVDF membrane after transformation of carboxyl groups to NHS-esters by EDC/NHS chemistry, and finally the Cys- and CysM-PAA-PVDF membrane. Water permeability of the thiol membranes was measured with a laboratory-scale stainless steel pressure cell (Sepa ST, GE Osmonics, effective membrane area 13.2 cm^2) in dead-end mode. This approach allows convective flow of the permeate through a membrane. The permeability experiment was performed according to our protocol described elsewhere.[28,66] The permeability of a PVDF membrane was measured after each step of the functionalization until the desired thiol membrane was formed.

4.6. Measurement of Adsorbed Cations in Functionalized Membranes. Synthetic water samples containing one cation per solution (Ca^{2+}, Hg^{2+}, Ag^{+}) and spiked wastewater samples containing multiple cations were passed through the thiol membranes by a convective flow process to (1) understand the transport mechanisms, (2) measure the cationic adsorption capacities, and (3) measure the HgS NP removal effectiveness. Silver (Ag^{+}) containing synthetic water was used to quantify the metal adsorption capacity of the thiol membranes, based on the assumption that Ag^{+} attaches to thiol groups in a 1:1 molar ratio. Samples of feeds, permeates, and retentates were acidified with nitric acid (1% v/v) and analyzed for Ca^{2+}, Hg^{2+}, and Ag^{+} concentrations using inductively coupled plasma optical emission spectroscopy (ICP-OES, VARIAN VISTA-PRO). For Ca^{2+} and Hg^{2+} analysis, the ICP-OES was calibrated from 0.5 to 100 ppm and from 0.5 to 1 ppm, respectively. For Ag^{+} analysis, the ICP-OES was calibrated in three different ranges of 0.1 to 1 ppm, 5 to 100 ppm, and 10 to 100 ppm, depending on the starting Ag^{+} concentration in the solution. Hg^{2+} concentrations were also measured by direct injection in a Nippon Instruments Corp. (NIC) MA-3000 analyzer. The MA-3000 was calibrated in the 1 to 100 ppb range. A material balance for the three cations

https://dx.doi.org/10.1021/acsomega.0c02526
ACS Omega 2020, 5, 22255−22267

enabled calculation of the removal and adsorption capacity of the thiol membranes.

■ ASSOCIATED CONTENT

Supporting Information

The Supporting Information is available free of charge at https://pubs.acs.org/doi/10.1021/acsomega.0c02526.

Industrial wastewater quality (S1) (Table S1); proposed treatment process to remove mercury from wastewater (S2) (Figure S1); primary filtration to remove particulates from wastewater using PVDF membrane (S3) (Figure S2); detail data of the membrane used for HgS nanoparticle separation (Table S2); ATR-FTIR spectra analysis of functionalized membranes (S4) (Figure S3); reaction steps of thiol membrane (S5) (Figure S4); adsorption−desorption study of Ag^{+} and Hg^{2+} cations on the PAA-PVDF membrane (S6) (Figure S5); adsorption efficiency of heavy metals on thiol membrane (S7) (Figure S6); mercury adsorption analysis on the CysM-PAA-PVDF membrane by XPS (S8) (Figure S7); results of EDX analysis of the CysM-PAA-PVDF membrane (S9) (Figure S8); summary of the EDX scanning results for the top surface of CysM-PAA-PVDF membrane (Table S3); materials (S10); EDC/NHS functionalization of the PAA-PVDF membrane and flux pattern (S11) (Figure S9); and cysteamine incorporation in NHS-PAA-PVDF membrane and flux pattern (S12) (Figure S10) (PDF)

■ AUTHOR INFORMATION

Corresponding Author

Dibakar Bhattacharyya − *Department of Chemical and Materials Engineering, University of Kentucky, Lexington, Kentucky 40506, United States;* orcid.org/0000-0001-9948-9085; Email: db@uky.edu

Authors

Mohammad Saiful Islam − *Department of Chemical and Materials Engineering, University of Kentucky, Lexington, Kentucky 40506, United States*

Ronald J. Vogler − *Department of Chemical and Materials Engineering, University of Kentucky, Lexington, Kentucky 40506, United States;* orcid.org/0000-0002-8683-9100

Sayed Mohammad Abdullah Al Hasnine − *Department of Mechanical Engineering, University of Kentucky, Lexington, Kentucky 40506, United States*

Sebastián Hernández − *Department of Chemical and Materials Engineering, University of Kentucky, Lexington, Kentucky 40506, United States;* orcid.org/0000-0002-7513-5511

Nga Malekzadeh − *Chevron Energy Technology Company, Richmond, California 94802, United States*

Thomas P. Hoelen − *Chevron Energy Technology Company, Richmond, California 94802, United States*

Evan S. Hatakeyama − *Chevron Energy Technology Company, Richmond, California 94802, United States*

Complete contact information is available at: https://pubs.acs.org/10.1021/acsomega.0c02526

Notes

The authors declare no competing financial interest.

■ ACKNOWLEDGMENTS

This work is supported by Chevron Energy Technology Co., Richmond, CA, and by the National Institute of Environmental Health Sciences (NIH-NIEHS-SRC) (grant P42ES007380) and by NSF-EPSCoR (Grant 1355438). We thank Dr. Gregory V. Lowry, Carnegie Mellon University, Pittsburgh, PA for providing the suspension of HgS nanoparticles. We thank Michael J. Detisch (graduate student) of the Department of Chemical and Materials Engineering, University of Kentucky (UK) for his support during XPS and EDS analysis. We also thank Dr. Nicolas Briot of Electron Microscopy Center (EMC), UK for his support to prepare samples for the FIB instrument as well as to analyze FIB samples. We also express our gratitude to Hongyi Wan (graduate student) of the Department of Chemical and Materials Engineering, UK for supporting us to explain FIB characterization data. We thank Md Ariful Hoque (graduate student) of Professor Marcelo Guzman's research group, Department of Chemistry, UK to support us to conduct (ATR-FTIR) experiments. We also express our sincere gratitude to Namal Wanninayake and Nadeesha Lakmali Kothalwala (graduate students) of Professor Doo Young Kim's research group, Department of Chemistry, UK for helping us to conduct (ATR-FTIR) experiments. Finally, we also acknowledge the support of Megan Combs of Environmental Research Training Laboratory (ERTL), UK for ICP-OES analytical assistance.

■ REFERENCES

(1) Arshadi, M.; Mousavinia, F.; Khalafi-Nezhad, A.; Firouzabadi, H.; Abbaspourrad, A. Adsorption of Mercury Ions from Wastewater by a Hyperbranched and Multi-Functionalized Dendrimer Modified Mixed-Oxides Nanoparticles. *J. Colloid Interface Sci.* **2017**, *505*, 293−306.

(2) Sun, M.; Cheng, G.; Ge, X.; Chen, M.; Wang, C.; Lou, L.; Xu, X. Aqueous Hg(II) Immobilization by Chitosan Stabilized Magnetic Iron Sulfide Nanoparticles. *Sci. Total Environ.* **2018**, *621*, 1074−1083.

(3) Sun, N.; Wen, X.; Yan, C. Adsorption of Mercury Ions from Wastewater Aqueous Solution by Amide Functionalized Cellulose from Sugarcane Bagasse. *Int. J. Biol. Macromol.* **2018**, *108*, 1199−1206.

(4) Saraydın, D.; Yıldırım, E. Ş.; Karadağ, E.; Güven, O. Radiation-Synthesized Acrylamide/Crotonic Acid Hydrogels for Selective Mercury (II) Ion Adsorption. *Adv. Polym. Technol.* **2018**, *37*, 822−829.

(5) Bansal, M.; Ram, B.; Chauhan, G. S.; Kaushik, A. L-Cysteine Functionalized Bagasse Cellulose Nnanofibers for Mercury(II) Ions Adsorption. *Int. J. Biol. Macromol.* **2018**, *112*, 728−736.

(6) Qin, H.; Xiao, R.; Guo, L.; Meng, J.; Chen, J. Mercury (II) Adsorption from Aqueous Solution using Nitrogen and Sulfur Co-Doped Activated Carbon. *Water Sci. Technol.* **2018**, *2017*, 310−318.

(7) Deng, S.; Zhang, G.; Liang, S.; Wang, P. Microwave Assisted Preparation of Thio-Functionalized Polyacrylonitrile Fiber for the Selective and Enhanced Adsorption of Mercury and Cadmium from Water. *ACS Sustainable Chem. Eng.* **2017**, *5*, 6054−6063.

(8) Bolisetty, S.; Peydayesh, M.; Mezzenga, R. Sustainable Technologies for Water Purification from Heavy Metals: Review and Analysis. *Chem. Soc. Rev.* **2019**, *48*, 463−487.

(9) AlOmar, M. K.; Alsaadi, M. A.; Jassam, T. M.; Akib, S.; Ali Hashim, M. Novel Deep Eutectic Solvent-Functionalized Carbon Nanotubes Adsorbent for Mercury Removal from Water. *J. Colloid Interface Sci.* **2017**, *497*, 413−421.

(10) Kokkinos, E.; Simeonidis, K.; Pinakidou, F.; Katsikini, M.; Mitrakas, M. Optimization of Tetravalent Manganese Feroxyhyte's Negative Charge Density: A High-Performing Mercury Adsorbent from Drinking Water. *Sci. Total Environ.* **2017**, *574*, 482−489.

(11) Gu, B.; Bian, Y.; Miller, C. L.; Dong, W.; Jiang, X.; Liang, L. Mercury Reduction and Complexation by Natural Organic Matter in Anoxic Environments. *Proc. Natl. Acad. Sci. U. S. A.* **2011**, *108*, 1479−1483.
(12) Ai, K.; Ruan, C.; Shen, M.; Lu, L. MoS_2 Nanosheets with Widened Interlayer Spacing for High-Efficiency Removal of Mercury in Aquatic Systems. *Adv. Funct. Mater.* **2016**, *26*, 5542−5549.
(13) Zhou, J.; Liu, Y.; Zhou, X.; Ren, J.; Zhong, C. Removal of Mercury Ions from Aqueous Solution by Thiourea-Functionalized Magnetic Biosorbent: Preparation and Mechanism Study. *J. Colloid Interface Sci.* **2017**, *507*, 107−118.
(14) Dąbrowski, A.; Hubicki, Z.; Podkościelny, P.; Robens, E. Selective Removal of The Heavy Metal Ions from Waters and Industrial Wastewaters by Ion-Exchange Method. *Chemosphere* **2004**, *56*, 91−106.
(15) Huang, L.; Peng, C.; Cheng, Q.; He, M.; Chen, B.; Hu, B. Thiol-Functionalized Magnetic Porous Organic Polymers for Highly Efficient Removal of Mercury. *Ind. Eng. Chem. Res.* **2017**, *56*, 13696−13703.
(16) Cheng, J.; Li, Y.; Li, L.; Lu, P.; Wang, Q.; He, C. Thiol-/Thioether-Functionalized Porous Organic Polymers for Simultaneous Removal of Mercury(II) Ion and Aromatic Pollutants in Water. *New J. Chem.* **2019**, *43*, 7683−7693.
(17) Thakur, S.; Das, G.; Raul, P. K.; Karak, N. Green One-Step Approach to Prepare Sulfur/Reduced Graphene Oxide Nanohybrid for Effective Mercury Ions Removal. *J. Phys. Chem. C* **2013**, *117*, 7636−7642.
(18) Ma, L.; Wang, Q.; Islam, S. M.; Liu, Y.; Ma, S.; Kanatzidis, M. G. Highly Selective and Efficient Removal of Heavy Metals by Layered Double Hydroxide Intercalated with the MoS_4^{2-} Ion. *J. Am. Chem. Soc.* **2016**, *138*, 2858−2866.
(19) Aguila, B.; Sun, Q.; Perman, J. A.; Earl, L. D.; Abney, C. W.; Elzein, R.; Schlaf, R.; Ma, S. Efficient Mercury Capture Using Functionalized Porous Organic Polymer. *Adv. Mater.* **2017**, *29*, 1700665.
(20) Bandaru, N. M.; Reta, N.; Dalal, H.; Ellis, A. V.; Shapter, J.; Voelcker, N. H. Enhanced Adsorption of Mercury Ions on Thiol Derivatized Single Wall Carbon Nanotubes. *J. Hazard. Mater.* **2013**, *261*, 534−541.
(21) Rudd, N. D.; Wang, H.; Fuentes-Fernandez, E. M. A.; Teat, S. J.; Chen, F.; Hall, G.; Chabal, Y. J.; Li, J. Highly Efficient Luminescent Metal−Organic Framework for the Simultaneous Detection and Removal of Heavy Metals from Water. *ACS Appl. Mater. Interfaces* **2016**, *8*, 30294−30303.
(22) Smuleac, V.; Butterfield, D. A.; Sikdar, S. K.; Varma, R. S.; Bhattacharyya, D. Polythiol-Functionalized Alumina Membranes for Mercury Capture. *J. Membr. Sci.* **2005**, *251*, 169−178.
(23) Gai, K.; Avellan, A.; Hoelen, T. P.; Lopez-Linares, F.; Hatakeyama, E. S.; Lowry, G. V. Impact of Mercury Speciation on Its Removal from Water by Activated Carbon and Organoclay. *Water Res.* **2019**, *157*, 600−609.
(24) Hernández, S.; Islam, M. S.; Thompson, S.; Kearschner, M.; Hatakeyama, E.; Malekzadeh, N.; Hoelen, T.; Bhattacharyya, D. Thiol-Functionalized Membranes for Mercury Capture from Water. *Ind. Eng. Chem. Res.* **2020**, *59*, 5287−5295.
(25) Hernández, S.; Lei, S.; Rong, W.; Ormsbee, L.; Bhattacharyya, D. Functionalization of Flat Sheet and Hollow Fiber Microfiltration Membranes for Water Applications. *ACS Sustainable Chem. Eng.* **2016**, *4*, 907−918.
(26) Wan, H.; Islam, M. S.; Briot, N. J.; Schnobrich, M.; Pacholik, L.; Ormsbee, L.; Bhattacharyya, D. Pd/Fe Nanoparticle Integrated PMAA-PVDF Membranes for Chloro-Organic Remediation from Synthetic and Site Groundwater. *J. Membr. Sci.* **2020**, *594*, 117454.
(27) Islam, M. S.; Hernández, S.; Wan, H.; Ormsbee, L.; Bhattacharyya, D. Role of Membrane Pore Polymerization Conditions for pH Responsive Behavior, Catalytic Metal Nanoparticle Synthesis, and PCB Degradation. *J. Membr. Sci.* **2018**, *555*, 348−361.
(28) Sarma, R.; Islam, M. S.; Miller, A.-F.; Bhattacharyya, D. Layer-by-Layer-Assembled Laccase Enzyme on Stimuli-Responsive Membranes for Chloro-Organics Degradation. *ACS Appl. Mater. Interfaces* **2017**, *9*, 14858−14867.
(29) Sarma, R.; Islam, M. S.; Running, M.; Bhattacharyya, D. Multienzyme Immobilized Polymeric Membrane Reactor for the Transformation of a Lignin Model Compound. *Polymers* **2018**, *10*, 463.
(30) Aher, A.; Thompson, S.; Nickerson, T.; Ormsbee, L.; Bhattacharyya, D. Reduced Graphene Oxide−Metal Nanoparticle Composite Membranes for Environmental Separation and Chloro-Organic Remediation. *RSC Adv.* **2019**, *9*, 38547−38557.
(31) Anari, Z.; Sengupta, A.; Sardari, K.; Wickramasinghe, S. R. Surface Modification of PVDF Membranes for Treating Produced Waters by Direct Contact Membrane Distillation. *Sep. Purif. Technol.* **2019**, *224*, 388−396.
(32) Zin, G.; Wu, J.; Rezzadori, K.; Petrus, J. C. C.; Di Luccio, M.; Li, Q. Modification of Hydrophobic Commercial PVDF Microfiltration Membranes into Superhydrophilic Membranes by the Mussel-inspired Method with Dopamine and Polyethyleneimine. *Sep. Purif. Technol.* **2019**, *212*, 641−649.
(33) Conde, J.; Dias, J. T.; Grazú, V.; Moros, M.; Baptista, P. V.; de la Fuente, J. M. Revisiting 30 Years of Biofunctionalization and Surface Chemistry of Inorganic Nanoparticles for Nanomedicine. *Front. Chem.* **2014**, *2*, 48.
(34) Wang, C.; Yan, Q.; Liu, H.-B.; Zhou, X.-H.; Xiao, S.-J. Different EDC/NHS Activation Mechanisms between PAA and PMAA Brushes and the Following Amidation Reactions. *Langmuir* **2011**, *27*, 12058−12068.
(35) Sam, S.; Touahir, L.; Andresa, J. S.; Allongue, P.; Chazalviel, J.-N.; Gouget-Laemmel, A. C.; de Villeneuve, C. H.; Moraillon, A.; Ozanam, F.; Gabouze, N.; Djebbar, S. Semiquantitative Study of the EDC/NHS Activation of Acid Terminal Groups at Modified Porous Silicon Surfaces. *Langmuir* **2010**, *26*, 809−814.
(36) Schuster, E. The Behavior of Mercury in the Soil with Special Emphasis on Complexation and Adsorption Processes - A Review of the Literature. *Water, Air, Soil Pollut.* **1991**, *56*, 667−680.
(37) Wagner-döbler, I. Pilot Plant for Bioremediation of Mercury-containing Industrial Wastewater. *Appl. Microbiol. Biotechnol.* **2003**, *62*, 124−133.
(38) Riauba, L.; Niaura, G.; Eicher-Lorka, O.; Butkus, E. A Study of Cysteamine Ionization in Solution by Raman Spectroscopy and Theoretical Modeling. *J. Phys. Chem. A* **2006**, *110*, 13394−13404.
(39) Besouw, M.; Masereeuw, R.; van den Heuvel, L.; Levtchenko, E. Cysteamine: An Old Drug with New Potential. *Drug Discovery Today* **2013**, *18*, 785−792.
(40) Gallego-Villar, L.; Hannibal, L.; Häberle, J.; Thöny, B.; Ben-Omran, T.; Nasrallah, G. K.; Dewik, A.-N.; Kruger, W. D.; Blom, H. J. Cysteamine Revisited: Repair of Arginine to Cysteine Mutations. *J. Inherited Metab. Dis.* **2017**, *40*, 555−567.
(41) Atwood, D. A.; Zaman, M. K. Mercury Removal from Water. In *Recent Developments in Mercury Science*; Atwood, D. A., Ed. Springer: Berlin, Heidelberg, 2005; Vol. *120*, pp. 163−182.
(42) Ritchie, S. M. C.; Bachas, L. G.; Olin, T.; Sikdar, S. K.; Bhattacharyya, D. Surface Modification of Silica- and Cellulose-Based Microfiltration Membranes with Functional Polyamino Acids for Heavy Metal Sorption. *Langmuir* **1999**, *15*, 6346−6357.
(43) Ritchie, S. M. C.; Kissick, K. E.; Bachas, L. G.; Sikdar, S. K.; Parikh, C.; Bhattacharyya, D. Polycysteine and Other Polyamino Acid Functionalized Microfiltration Membranes for Heavy Metal Capture. *Environ. Sci. Technol.* **2001**, *35*, 3252−3258.
(44) Ladhe, A. R.; Frailie, P.; Hua, D.; Darsillo, M.; Bhattacharyya, D. Thiol-Functionalized Silica-Mixed Matrix Membranes for Silver Capture from Aqueous Solutions: Experimental Results and Modeling. *J. Membr. Sci.* **2009**, *326*, 460−471.
(45) Bolisetty, S.; Mezzenga, R. Amyloid−carbon Hybrid Membranes for Universal Water Purification. *Nat. Nanotechnol.* **2016**, *11*, 365−371.
(46) French, R. A.; Jacobson, A. R.; Kim, B.; Isley, S. L.; Penn, R. L.; Baveye, P. C. Influence of Ionic Strength, pH, and Cation Valence on

https://dx.doi.org/10.1021/acsomega.0c02526
ACS Omega 2020, 5, 22255−22267

Aggregation Kinetics of Titanium Dioxide Nanoparticles. *Environ. Sci. Technol.* **2009**, *43*, 1354−1359.
(47) Liu, G.; Cai, Y.; O'Driscoll, N. *Environmental Chemistry and Toxicology of Mercury*; John Wiley & Sons: 2011.
(48) Powell, K. J.; Brown, P. L.; Byrne, R. H.; Gajda, T.; Hefter, G.; Sjöberg, S.; Wanner, H. Chemical Speciation of Hg(II) with Environmental Inorganic Ligands. *Aust. J. Chem.* **2004**, *57*, 993−1000.
(49) Humbert, H.; Gallard, H.; Suty, H.; Croué, J.-P. Natural Organic Matter (NOM) and Pesticides Removal Using a Combination of Ion Exchange Resin and Powdered Activated Carbon (PAC). *Water Res.* **2008**, *42*, 1635−1643.
(50) Luxbacher, T. Electrokinetics on Polymer Surfaces. In *9th Freiberger Polymertag*; Hüthig: 2009.
(51) Perrin, D. D.; Dempsey, B.; Serjeant, E. P. *pKa Prediction for Organic Acids and Bases*; Springer: Netherlands, 1981.
(52) Luxbacher, T. *The ZETA Guide: Principles of the Streaming Potential Technique*; First ed.; Anton Paar GmbH: Graz, Austria, 2014.
(53) Zhang, W.; Wahlgren, M.; Sivik, B. Membrane Characterization by the Contact Angle Technique: II. Characterization of UF-Membranes and Comparison Between the Captive Bubble and Sessile Drop as Methods to Obtain Water Contact Angles. *Desalination* **1989**, *72*, 263−273.
(54) Baek, Y.; Kang, J.; Theato, P.; Yoon, J. Measuring Hydrophilicity of RO Membranes by Contact Angles via Sessile Drop and Captive Bubble Method: A Comparative Study. *Desalination* **2012**, *303*, 23−28.
(55) Baes, C. F.; Mesmer, R. E. *The Hydrolysis of Cations*; John Wiley & Sons: New York, USA, 1976.
(56) Gai, K.; Hoelen, T. P.; Hsu-Kim, H.; Lowry, G. V. Mobility of Four Common Mercury Species in Model and Natural Unsaturated Soils. *Environ. Sci. Technol.* **2016**, *50*, 3342−3351.
(57) *National Primary Drinking Water Regulations*; https://www.epa.gov/ground-water-and-drinking-water/national-primary-drinking-water-regulations.
(58) Rahman, M. M.; Islam, M. S.; Rahman, M. A.; Tun, H.; Deshmane, V.; Hossain, T.; Ilias, S. Evaluation and Characterization of Pd-Ag Composite Membrane Fabricated by Surfactant Induced Electroless Plating (SIEP) for Hydrogen Separation. *Sep. Sci. Technol.* **2019**, *54*, 2084−2097.
(59) Islam, M. S.; Rahman, M. M.; Ilias, S. Characterization of Pd−Cu Membranes Fabricated by Surfactant Induced Electroless Plating (SIEP) for Hydrogen Separation. *Int. J. Hydrogen Energy* **2012**, *37*, 3477−3490.
(60) Finlayson, B. A. *Introduction to Chemical Engineering Computing*; Second ed.; Wiley-Interscience: 2006.
(61) Cussler, E. L. *Diffusion: Mass Transfer in Fluid Systems*; Third ed.; Cambridge University Press: 2009, DOI: 10.1017/CBO9780511805134.
(62) Southard, M. Z.; Green, D. W. *Perry's Chemical Engineers' Handbook*; Nineth ed.; McGraw-Hill Education: 2018.
(63) Hernández, S.; Papp, J. K.; Bhattacharyya, D. Iron-Based Redox Polymerization of Acrylic Acid for Direct Synthesis of Hydrogel/Membranes and Metal Nanoparticles for Water Treatment. *Ind. Eng. Chem. Res.* **2014**, *53*, 1130−1142.
(64) Bhattacharyya, D.; Schäfer, T.; Wickramasinghe, S. R.; Daunert, S. *Responsive Membranes and Materials*; Wiley: West Sussex, United Kingdom, 2013.
(65) Xiao, L.; Davenport, D. M.; Ormsbee, L.; Bhattacharyya, D. Polymerization and Functionalization of Membrane Pores for Water Related Applications. *Ind. Eng. Chem. Res.* **2015**, *54*, 4174−4182.
(66) Wan, H.; Briot, N. J.; Saad, A.; Ormsbee, L.; Bhattacharyya, D. Pore Functionalized PVDF Membranes with In-Situ Synthesized Metal Nanoparticles: Material Characterization, and Toxic Organic Degradation. *J. Membr. Sci.* **2017**, *530*, 147−157.

https://dx.doi.org/10.1021/acsomega.0c02526
ACS Omega 2020, 5, 22255−22267